J. Fluid Mech. (1967), *vol.* 28, *part* 4, *pp.* 643–655
Printed in great Britain

Steady flows in rectangular cavities

By FRANK PAN AND ANDREAS ACRIVOS
Department of Chemical Engineering, Stanford University

(Received 25 July 1966)

This paper deals with the steady flow in a rectangular cavity where the motion is driven by the uniform translation of the top wall. Creeping flow solutions for cavities having aspect ratios from $\frac{1}{4}$ to 5 were obtained numerically by a relaxation technique and were shown to compare favourably with Dean & Montagnon's (1949) similarity solution, as extended by Moffatt (1964), in the region near the bottom corners of a square cavity as well as throughout the major portion of a cavity with aspect ratio equal to 5. In addition, for a Reynolds number range from 20 to 4000, flow patterns were determined experimentally by means of a photographic technique for finite cavities, as well as for cavities of effectively infinite depth. These experimental results suggest that, within finite cavities, the high Reynolds number steady flow should consist essentially of a single inviscid core of uniform vorticity with viscous effects being confined to thin shear layers near the boundaries, while, for cavities of infinite depth, the viscous and inertia forces should remain of comparable magnitude throughout the whole domain even in the limit of very large Reynolds number R.

1. Introduction

The motion generated in a fluid-filled rectangular cavity by the uniform translation of one of the walls (figure 1) represents one of the simplest examples of steady flow involving closed streamlines, and as such has occupied a position of considerable theoretical importance within the broader field of steady separated flows. Previous work on this topic has been reviewed in detail by Burggraf (1966), who, for the special case of a square cavity, also obtained numerical solutions to the full Navier–Stokes equations for a range of Reynolds number $R \equiv VD/\nu$ from 0 to 400 (V is the velocity of the top plate, D is the width of the cavity and ν is the kinematic viscosity of the fluid). From all these studies, as well as the recent one by Weiss & Florsheim (1965), one can obtain a fairly clear picture of the overall flow characteristics in this and related systems, and yet, upon closer examination, it becomes apparent that a number of basic questions regarding the more detailed structure of the flow still remain very much unsettled.

Perhaps the most important point along these lines relates to the steady flow behaviour in the limit of very low viscosity. This, as will be recalled, is an old subject, having been first considered by Prandtl (1904), who showed, as did Batchelor (1956), that the steady high Reynolds number flow within closed streamlines should consist of an inviscid core having uniform vorticity with viscous effects being confined to infinitesimally thin shear layers along the bound-

aries. This theorem, although of considerable theoretical interest, is, however, of limited practical value by itself in that, for many problems, the boundaries of the uniform vorticity core are unknown *a priori* and cannot be located from basic principles alone without a detailed solution of the full equations of motion. For example, in the case of a square cavity, one can immediately think of at least two

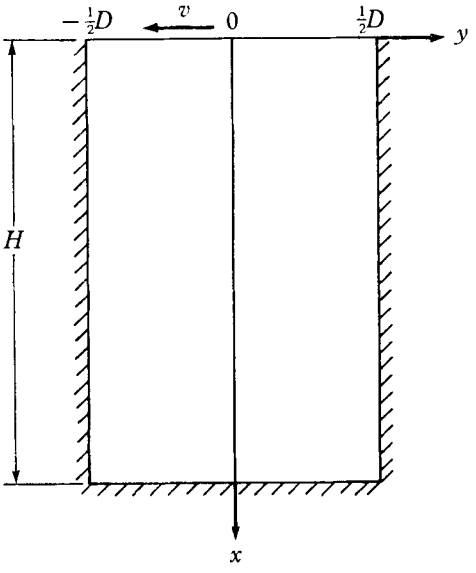

FIGURE 1. A sketch of the co-ordinate system in a rectangular cavity.

possibilities: either one could assume that the boundaries of the core would have to coincide with the solid walls of the cavity; or, in view of Burggraf's (1966) numerical results that show, at $R = 400$, a flow consisting of a primary eddy plus two secondary eddies† appearing in the bottom corners of the cavity, one could suppose that the limiting flow as $R \to \infty$ would also possess this same feature and thus consist of at least three distinct inviscid cores, each with its own (uniform) vorticity. Clearly, from what is known so far, one has little basis for choosing between these two alternatives.

An even more fundamental question arises, however, concerning the steady high Reynolds number flow in a cavity having effectively an infinite aspect ratio $A \equiv H/D$. From experimental observations it is known that the motion here consists of a series of vortices superimposed upon one another, but what is not known is how the size, i.e. the maximum vertical dimension, of these eddies is affected by a continual increase in the Reynolds number R. Consider, for example, the primary vortex, i.e. the one closest to the moving wall. If one were sure that the size of this vortex would approach a finite limit as $R \to \infty$, then, of course, one could invoke the uniform vorticity theorem to describe the motion within its core. This, however, is by no means certain, and in fact it is quite conceivable that the size of this eddy could increase indefinitely with increasing R, in which case,

† These are in addition to the usual hierarchy of viscous corner eddies described by Moffatt (1964).

that is if it were found that the viscous forces had an important bearing on the overall dimensions of the vortex, one would be forced to conclude that the core of the eddy could never become inviscid even in the limit $R \to \infty$. Thus, once again, one is faced with two fundamentally distinct possibilities regarding the steady high Reynolds number flow with very little basis for deciding between them.

In view of these unsettled questions it appeared desirable therefore to study anew this flow system for a wide range of Reynolds numbers and aspect ratios in the hope of, *inter alia*, providing answers to the points raised above. In this paper, we shall first present numerical solutions to the creeping-flow equations for aspect ratios from 0·25 to 5, paying particular attention to the comparison between these numerical results and Moffatt's (1964) similarity solution for flow near a sharp corner. Following this, we shall describe the principal features of an experimental investigation in which the Reynolds number was varied from 18 to approximately 4000. And, finally, we shall show how these experimental results can lead to important conclusions regarding the nature of the steady flow in the limit $R \to \infty$.

2. Creeping-flow solution

In the absence of the inertia terms, the equations of motion reduce to the familiar biharmonic equation $\nabla^4 \psi = 0,$

where ψ is the dimensionless stream function, with boundary conditions:

$$\psi = 0 \text{ on all four boundaries,}$$
$$\partial\psi/\partial X = 1 \quad \text{at} \quad X = 0; \quad \partial\psi/\partial X = 0 \quad \text{at} \quad X = A \equiv H/D,$$
$$\partial\psi/\partial Y = 0 \quad \text{at} \quad Y = \pm\tfrac{1}{2}.$$

As already remarked by Burggraf (1966), the form of the boundary conditions precludes an analytic solution of this system by one of the standard procedures used successfully in the field of elasticity. Also, approximate methods, such as the variational technique (Weiss & Florsheim 1965) and Galerkin's method (Snyder, Spriggs & Stewart 1964), are not refined enough for our purposes in that, besides their uncertain accuracy, they do not bring out some of the more interesting features of the solution to be described shortly. The problem was therefore treated numerically by means of the relaxation procedure employed by Burggraf (1966).

Streamline patterns for rectangular cavities with aspect ratios $A = 0{\cdot}25$, 0·50, 1·0, 2·0 and 5·0 are shown in figure 2. These complement the earlier results of Kawaguti (1961) for aspect ratios $\frac{1}{2}$, 1 and 2, which, unfortunately, are somewhat inaccurate owing to his rather coarse mesh size. It is interesting to note, from figure 2, that the pattern in the primary vortex when $A = 2$ is practically identical to that when $A = 5$, implying that the flow in the primary eddy remains unaffected by the location of the bottom wall as long as $A > 2$. The locations of the vortex centres are presented in table 1. It is somewhat surprising that these compare quite favourably with Weiss & Florsheim's (1965) approximate results even though the latter were obtained for a system with a different boundary condition at $X = 0$.

It is instructive at this point to compare our numerical results with two rather

simple asymptotic solutions that can be derived analytically. The first of these applies in the limit $A \to 0$ where, in view of the fact that the streamlines become essentially parallel to the y-axis over most of the region inside the cavity, the expression for the stream-function reduces to

$$\psi = X(1-X/A)^2.$$

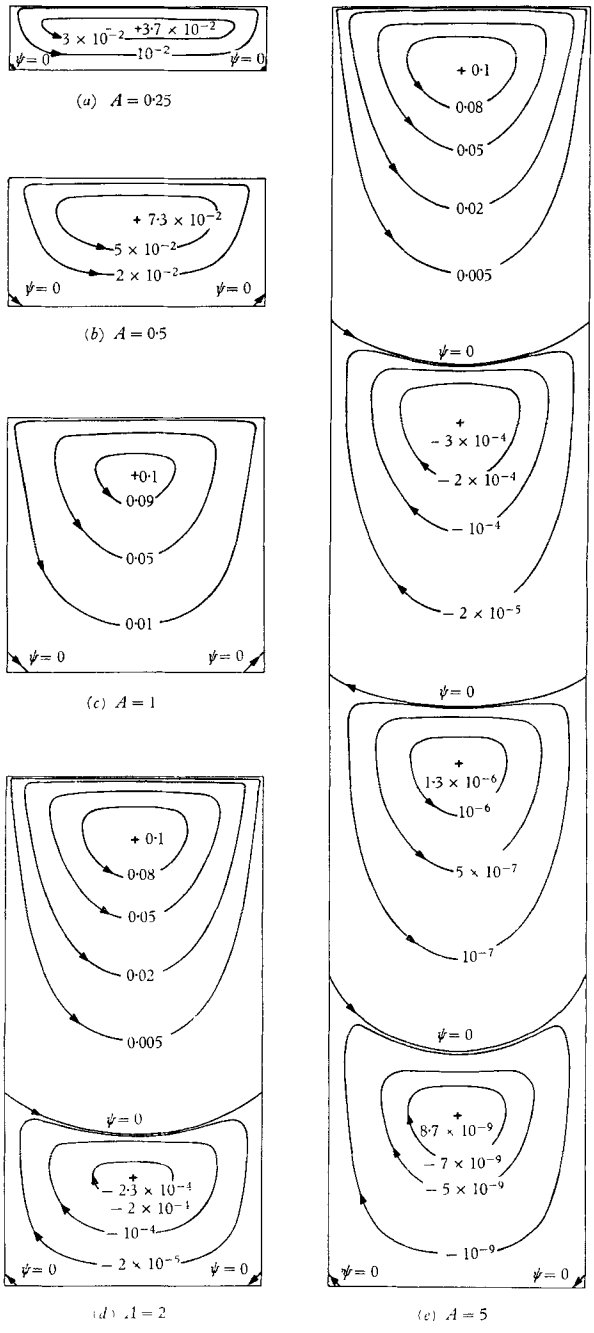

FIGURE 2. Creeping-flow streamline patterns in rectangular cavities.

From this one obtains that, at the vortex centre, $\psi = 0{\cdot}148A$ and $X = \frac{1}{3}A$, which as seen from figure 2 and table 1 is in excellent agreement with the corresponding values from the numerical results, pertaining to $A = \frac{1}{4}$ and $A = \frac{1}{2}$.

The second analytical solution,

$$\psi = r^{\lambda}\{a\cos\lambda\theta + b\cos(\lambda - 2)\theta\}, \tag{1}$$

where r and θ are the usual polar co-ordinates, is due to Dean & Montagnon (1949) and describes the viscous flow very near the apex ($r = 0$) of a corner with angle 2α. As shown by Moffatt (1964), complex values of λ, which arise whenever $2\alpha < 146°$, imply the existence of an infinite set of vortices of diminishing size and rapidly decreasing strength as $r \to 0$.

		Vortex centre x/D			
$A \equiv H/D$	h (mesh size)	1st	2nd	3rd	4th
0·25	0·0125	0·0875	—	—	—
0·50	0·0125	0·1628	—	—	—
1·0	0·01	0·24†	—	—	—
2·0	0·025	0·25	1·575	—	—
5·0	0·025	0·25	1·625	2·95	4·31

TABLE 1. Numerically determined vortex centre locations in creeping flow (†Burggraf (1966) obtained the same result with $h = 0{\cdot}025$).

The special case $2\alpha \to 0$ corresponds to the flow between two parallel flat plates, which, according to the appropriate form of the similarity solution, should consist of an infinite set of vortices all having a length to width ratio equal to 1·39. This prediction, although based on a solution which is supposed to hold only asymptotically far away from the moving wall, is borne out to a surprising degree by our numerical results for the case $A = 5$, which show (cf. figure 2) the first three vortices as having a length to width ratio equal to 1·40.

The flow in the corner region of a square cavity ($A = 1$) offers another opportunity for comparing the numerical results with the similarity solution, in this case with $2\alpha = \frac{1}{2}\pi$. At first difficulties were encountered because even a mesh size h as small as 0·01, although more than adequate for obtaining the solution in the core of the cavity, was found to be still too coarse to reveal the detailed streamline pattern inside the corner eddies. Fortunately, it was soon observed that the solution in the core remained practically unaffected by changes in the structure of the corner vortices, which meant that an improved solution could be computed simply once convergence in the core was assured by subdividing the region around the corners into finer meshes and iterating further. This process of subdivision was repeated several times and disclosed a sequence of eddies, as shown in figure 3, which were amazingly similar and symmetric with respect to the diagonal of the square cavity. Table 2 lists the relative sizes and strengths of these corner vortices together with the respective analytical results obtained by Moffatt (1964) from the similarity solution. Once again there is excellent agreement between the two sets, implying that Moffatt's solution remains valid not only as the apex of the

corner is approached, but throughout the region within which the corner vortices are contained. It is worth noting though that this region occupies only about 0·5 % of the total area of the square cavity.

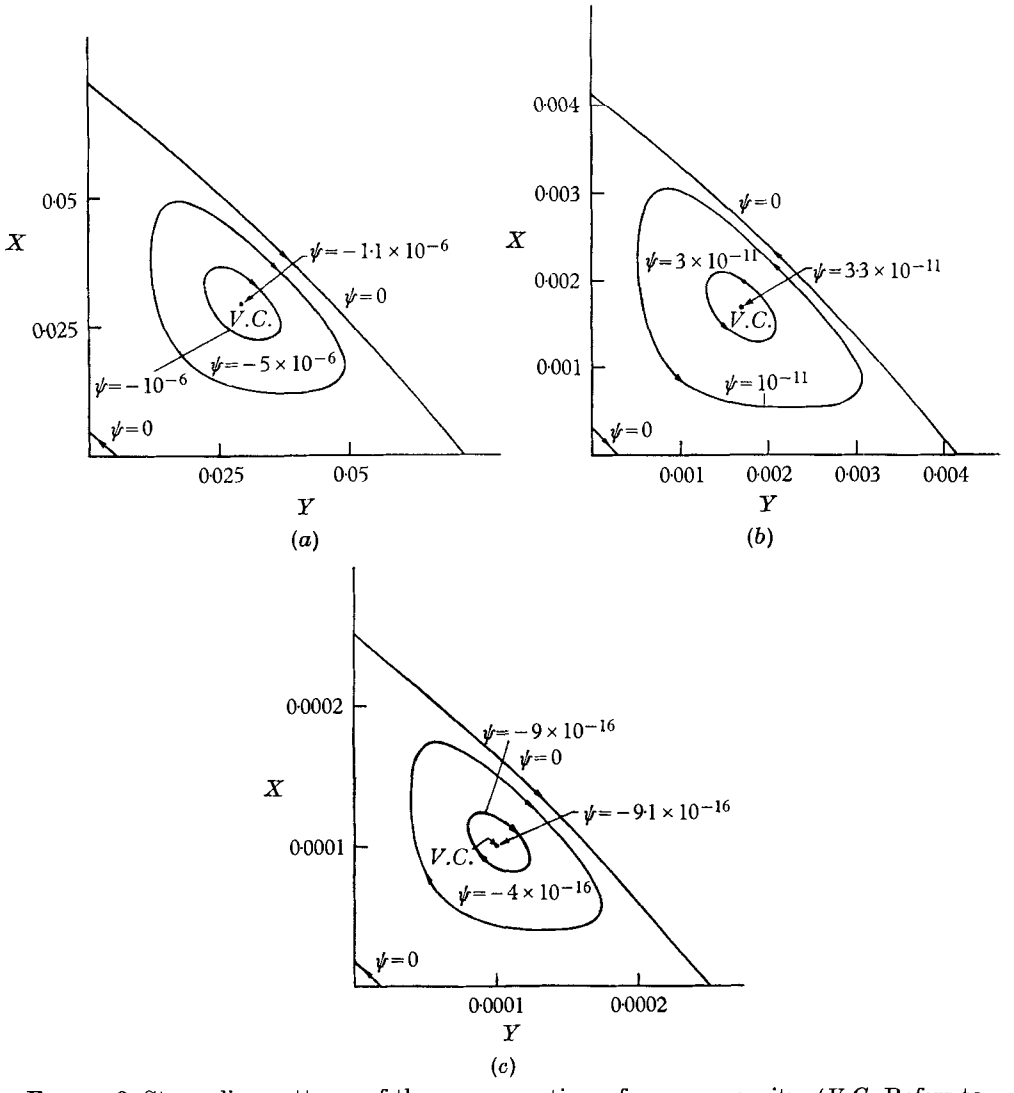

FIGURE 3. Streamline patterns of the corner vortices of a square cavity. (*V.C.* Refers to vortex centre.)

		r_n	r_n/r_{n+1}	$v_{n-\frac{1}{2}}$	$v_{n-\frac{1}{2}}/v_{n+\frac{1}{2}}$
Moffatt's solution		—	16·4	—	2070
Numerical solution	1st corner vortex	$4{\cdot}16 \times 10^{-2}$	16·4	$2{\cdot}06 \times 10^{-4}$	2170
	2nd corner vortex	$2{\cdot}54 \times 10^{-3}$		$9{\cdot}50 \times 10^{-8}$	
	3rd corner vortex	$1{\cdot}52 \times 10^{-4}$	16·7	$4{\cdot}50 \times 10^{-11}$	2110

TABLE 2. The relative sizes and strengths of the corner vortices in the square cavity (r_n denotes the distance from the apex to the centre of the nth vortex, while $v_{n-\frac{1}{2}}$ is the velocity at the intersection of the 45° line and the dividing streamline between the nth and the $(n-1)$th vortices).

By fitting the numerical results to (1) it was also found possible to determine approximate values for the coefficients a and b. This in turn gave the two expressions:

for $A \gg 1$,

$$\psi \cong 0{\cdot}3\,e^{-4{\cdot}21X}\{e^{-2{\cdot}26Y}[\cos(1{\cdot}4-2{\cdot}26X+4{\cdot}21Y)+1{\cdot}8Y\cos(1{\cdot}22-2{\cdot}26X+4{\cdot}21Y)] + e^{2{\cdot}26Y}[\cos(1{\cdot}4-2{\cdot}26X-4{\cdot}21Y)-1{\cdot}8Y\cos(1{\cdot}22-2{\cdot}26X+4{\cdot}21Y)]\}$$

within that portion of the flow outside the primary vortex;

for $A = 1$,

$$\psi \cong 0{\cdot}15r^{3{\cdot}74}\{e^{1{\cdot}13\theta}[\cos(0{\cdot}88-3{\cdot}74\theta+1{\cdot}13\ln r)+1{\cdot}39\cos(2{\cdot}3-1{\cdot}74\theta+1{\cdot}13\ln r)] + e^{-1{\cdot}13\theta}[\cos(0{\cdot}88-3{\cdot}74\theta+1{\cdot}13\ln r)+1{\cdot}39\cos(2{\cdot}3-1{\cdot}74\theta+1{\cdot}13\ln r)]\}$$

within the region containing corner vortices.

Although the numerical calculations can be extended in principle to include inertial effects, serious instabilities in the numerical procedure seem to set in for $R > 400$ (Burggraf 1966) which invalidate the results. Hence, in order to continue the investigation, it was found necessary to set up the experimental program described in the next section which covered the range of Reynolds numbers between 20 and 4000. As will be shown, in addition to complementing the theoretical solutions, these experimental results will lead to important and in some respects surprising conclusions about the basic features of the steady flow as $R \to \infty$.

3. Experimental techniques and results

As shown in figure 4, the apparatus consisted of a rotating wheel 12 in. in diameter which was placed on top of a rectangular cavity having a width of 4 in., a height of 40 in. and a span of 4 in. The walls of the cavity were made of plexiglass to facilitate visual observation from all directions. Also, the aspect ratio was set to any desired value by merely inserting a removable bottom which was then held in position by a pair of magnets placed outside the walls. Of course, the curvature of the wheel altered the shape of the top boundary from that considered in the mathematical model, but it was felt that except for very shallow cavities this modification was not sufficiently serious to warrant much concern. More bothersome was the unavoidable presence of three-dimensional fluid motions near the four intersections of the vertical sides. Although it was not possible to ascertain their influence on the overall flow pattern, it was observed that these motions did not extend into the mid-section, where to all appearances the flow was indeed two-dimensional. That is not to say that these wall effects were necessarily insignificant, but our observations did lead us to conclude that these effects were much less serious in our case than in the system studied by Maull & East (1963), where, under turbulent conditions, regular three-dimensional flows were noted

throughout the spanwise direction in cavities having large ratios of span-to-chord.

The cavity was filled with a clear oil in which nitrogen-filled glass micro-spheres about 10^{-4}in. in diameter were added to serve as tracers. Since these micro-balloons rose very slowly and were too small to disturb the flow, their streaks on a time exposure picture gave a proper representation of the flow streamlines at steady state. The pictures were taken by focusing a large lens with a narrow depth of field (about 1 cm) on the mid-section, which was illuminated from the side by a

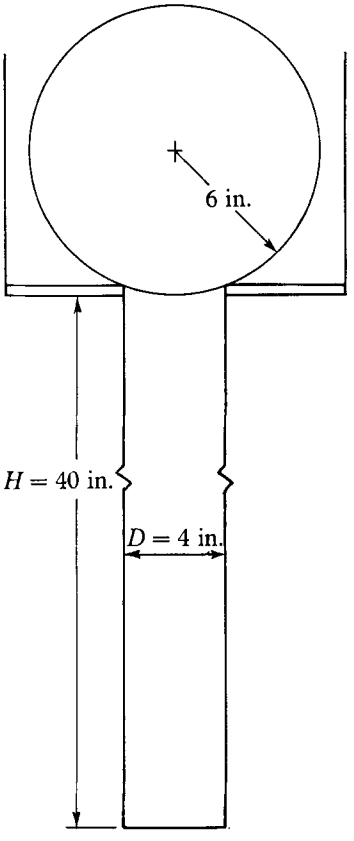

FIGURE 4. Experimental apparatus.

slit light source in order to improve the contrast between the tracer streaks and the background. In this way, using exposure times of up to 5 min, flows were even photographed which, as in the case of the corner eddies, were too slow to be observed visually. Typical streamline patterns are shown in figure 5, plate 1, depicting very clearly many of the principal features of the motion such as the location of the dividing streamlines and the centres of the vortices. The aspect ratios in the experiments ranged from $A = 0{\cdot}5$ to $A = 10$, but the majority of the experiments were performed with $A = 1{\cdot}0$, $1{\cdot}6$ and 10.

As explained in the introduction, one of the basic questions the present study intended to resolve was in regard to the nature of the steady flow as $R \to \infty$ both

for cavities with finite aspect ratios as well as for cavities of infinite depth. To this end, let us consider first the experimental results for a square cavity as well as those for a rectangular cavity having an aspect ratio A of 1·6, and in particular the size of the upstream corner vortex, i.e. the one appearing on the right half of figure 6, plate 2, as a function of the Reynolds number R. This size, which is defined as the fraction of the vertical wall covered by the upstream vortex, was determined quite accurately from the time exposures and, for the case of a square cavity, is seen plotted against R in figure 7. As is evident, this size was found

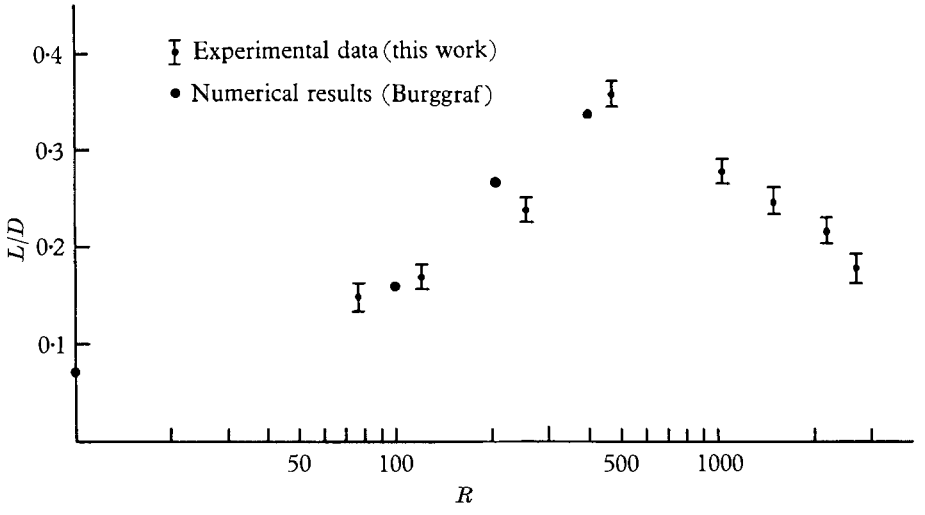

FIGURE 7. Size of the upstream corner vortex of a square cavity *vs.* Reynolds number.

to increase from a value of about 0·1 under creeping-flow conditions to a maximum of approximately 0·35 around $R = 500$, in excellent agreement with the results from Burggraf's (1966) numerical solution.† With a further increase in R, however, the upstream corner vortex began to shrink slowly, until at $R = 2700$ it was found to have retreated once again into the immediate neighbourhood of the cavity corner. This rather surprising behaviour of the upstream corner eddy is even more evident in the case of the rectangular cavity with $A = 1{\cdot}6$ and is shown in figure 8, plate 3.

The experiments in a cavity with aspect ratio 10, which was used as a model for a cavity having an infinite depth, were also very revealing. The flow here consisted of a series of vortices, superimposed on one another, the first three of which are shown in figure 9, plate 4, at $R \sim 3200$. In principle, of course, one should have expected many more vortices below the third, but owing to their extremely slow motion these could be neither observed nor photographed. As seen from figure 5, plate 1, the stagnation point of the streamline dividing the primary from the secondary eddy is well defined on the photographs and, hence, its distance from the moving wall, L/D, was chosen to represent the size of the primary vortex. The functional dependence of L/D on R is shown in figure 10.

† Figure 7 also includes a point at $L/D = 0{\cdot}267$ and $R = 200$ which was computed numerically by Professor Burggraf and communicated to the authors.

Once again, as with finite cavities, the primary vortex was found to shrink at first as R was increased from the creeping flow limit; but beyond a Reynolds number of approximately 800 the vortex was observed to grow, with its size seemingly becoming proportional to $R^{\frac{1}{2}}$ in the range of R between 1500 and 4000, at which point instabilities began to set in.

The picture that emerges then from these experimental investigations regarding the steady high Reynolds number flow is as follows.

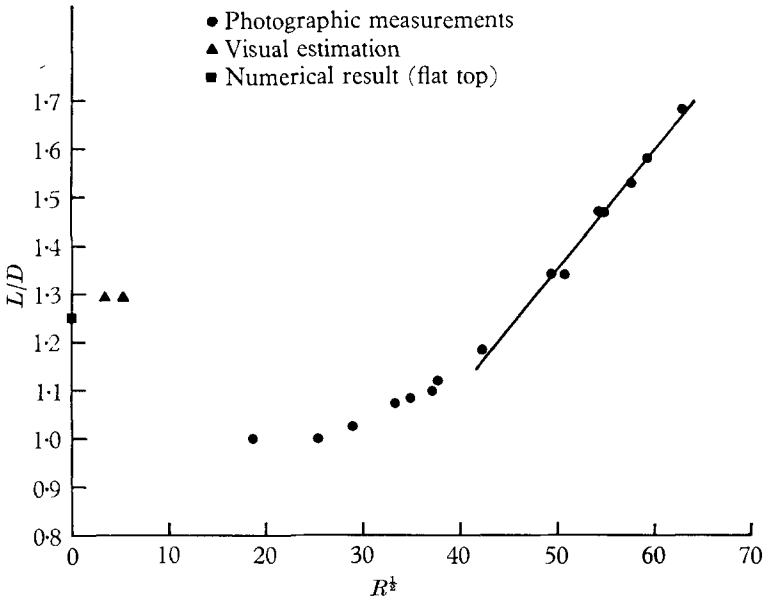

FIGURE 10. The stagnation-point position of the primary vortex in an infinite cavity *vs.* Reynolds number.

Finite cavities

The primary vortex will extend practically throughout the whole region of a cavity having a finite aspect ratio provided the Reynolds number is made sufficiently large, and, although the presence of the corner eddies cannot be completely discounted since it is not certain at present that these will truly vanish as $R \to \infty$, it is evident that at worst these will occupy only an insignificant portion of the total cavity. Hence, it would appear that to all intents and purposes the steady flow in the limit $R \to \infty$ will consist of a *single* inviscid core of uniform vorticity with viscous effects being confined to infinitesimally thin boundary layers along the walls.

This would mean, for example, that in the constant vorticity core of a cavity with a very small aspect ratio A

$$\psi = \tfrac{1}{2}\omega X(1 - X/A),$$

where, in view of the fact that the velocity outside the boundary layer is uniform, the constant vorticity ω can be computed simply from Batchelor's (1956) equation (3.6). This results in a value for ω equal to $\sqrt{2}$.

Cavities of infinite depth

The flow here is fundamentally different from that in the preceding case, in that the continual increase with R of the size of the primary vortex precludes its core from ever attaining an inviscid state even as $R \to \infty$, since in a truly inviscid vortex the streamline pattern should not of course be affected by changes in the value of the Reynolds number R. This seemingly paradoxical conclusion to the effect that viscous forces should somehow be included in the description of the flow even for vanishingly small viscosity will now be supported by a relatively simple theoretical argument.

Consider the primary eddy. It is known experimentally that, besides having a length which increases monotonically with R for $R > 1500$ this eddy also possesses a flow structure within its central part consisting of streamlines that are almost parallel to the x-axis. Therefore, in order to retain, even when $R \to \infty$, the viscous as well as the inertia terms along this central core, which incidentally extends throughout the major portion of the eddy, we can transform the usual dimensionless variables X, Y, u, v and p into the corresponding stretched quantities $\hat{x}$, $\hat{y}$, $\hat{u}$, $\hat{v}$ and $\hat{p}$ by means of

$$X = R^n \hat{x} \ (n > 0), \quad Y = \hat{y}, \quad u = R^{n-1}\hat{u}, \quad v = R^{-1}\hat{v} \quad \text{and} \quad p = R^{2(n-1)}\hat{p}. \tag{2}$$

Thus, in the limit $R \to \infty$, the Navier–Stokes equations reduce to

$$\hat{u}\frac{\partial \hat{u}}{\partial \hat{x}} + \hat{v}\frac{\partial \hat{u}}{\partial \hat{y}} = -\frac{\partial \hat{p}}{\partial \hat{x}} + \frac{\partial^2 \hat{u}}{\partial \hat{y}^2}, \quad \frac{\partial \hat{p}}{\partial \hat{y}} = 0, \tag{3}$$

together with the continuity equation $\partial \hat{u}/\partial \hat{x} + \partial \hat{v}/\partial \hat{y} = 0$. Equation (3) cannot remain valid of course in the region near the moving plate where the flow is mostly in the y-direction and v is $O(1)$. Here a typical boundary-layer-type analysis applies resulting in the familiar boundary-layer equation

$$\bar{u}\frac{\partial v}{\partial \bar{x}} + v\frac{\partial v}{\partial Y} = \frac{\partial^2 v}{\partial \bar{x}^2}, \tag{4}$$

with $\bar{u} = u\sqrt{R}$ and $\bar{x} = x\sqrt{R}$, and with boundary conditions

$$v = 1 \quad \text{at} \quad \bar{x} = 0, \quad v \to 0 \quad \text{as} \quad \bar{x} \to \infty.$$

Moreover, the requirement that this solution should match with that of (3) in the overlap domain $\bar{x} \to \infty$, $\hat{x} \to 0$ easily leads to the result than n must equal $\frac{1}{2}$ in (2).

This analysis appears to be consistent everywhere except near the two upper corners of the cavity, where it is not at all clear that a proper matching of our two solutions can be effected. For example, the analysis would require that a fluid element having a velocity v of $O(1)$ inside the boundary layer should be able to slow down to a velocity u of $O(R^{-\frac{1}{2}})$ upon turning the upper right corner; and, conversely, near the upper left corner, that the flow should be able to accelerate suddenly from a velocity u of $O(R^{-\frac{1}{2}})$ inside the viscous layer to a velocity v of $O(1)$ inside the boundary layer. Of course, these two corners in question represent singular regions where one would expect the high R flow to be extremely com-

plicated and to exhibit, possibly, the behaviour just outlined, but, obviously, this whole question needs to be studied further in much more detail.

With these reservations in mind then, our theoretical arguments would indicate, that the length of the primary vortex should become proportional to $\sqrt{R}$ for $R \gg 1$, a fact which, as remarked earlier, is borne out by the experimental observations. Another prediction is that the speed along the central portion should be $O(R^{-\frac{1}{2}})$. To test this, a series of velocity measurements† were

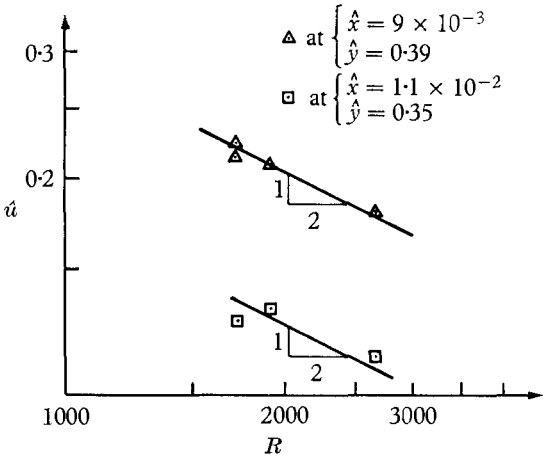

FIGURE 11. Stretched velocity $\hat{u}$ *vs.* Reynolds number.

undertaken using the stroboscopic air-bubble technique described by Grove (1963) with the results shown in figure 11. As can be seen, the data, although by necessity somewhat inaccurate owing to the low speeds involved, exhibit a trend with R which is in at least qualitative agreement with the theoretical predictions.

The analysis leading up to (2) and (3) can also be repeated for each region enclosed by any of the remaining vortices, but here the great difficulty in obtaining quantitative measurements of the velocities and the streamline patterns make any comparison between the experimental and theoretical results rather meaningless.

Finally, it is worth pointing out that the flow behaviour in a cavity having an infinite depth is qualitatively similar to that observed inside the steady circulating wake behind a cylinder (Acrivos, Snowden, Grove & Petersen 1965), where it was also concluded that the viscous and inertia forces had to remain of the same order of magnitude even in the limit $R \to \infty$. It would appear, therefore, that a steady eddy, which is not wholly artificially constrained in the manner, say, of a cavity with a finite aspect ratio, does not reach a finite size as the Reynolds number is increased but continues to enlarge itself in such a way that a proper balance between the viscous and the inertia effects is maintained throughout its core.

† Since the velocities have to be compared at the same point in the stretched coordinate system, many measurements were necessary before a few could be used.

This work was supported in part by grants from the National Science Foundation and the Chevron Research Corporation. The authors wish to record their indebtedness to Ricardo Levy, who performed many of the early preliminary experiments, and to D. D. Snowden and O. Burggraf for many constructive criticisms and helpful suggestions.

REFERENCES

Acrivos, A., Snowden, D. D., Grove, A. S. & Petersen, E. E. 1965 *J. Fluid Mech.* **21**, 737.

Batchelor, G. K. 1956 *J. Fluid Mech.* **1**, 177.

Burggraf, O. R. 1966 *J. Fluid Mech.* **24**, 113.

Dean, W. R. & Montagnon, P. E. 1949 *Proc. Camb. Phil. Soc.* **45**, 389.

Grove, A. S. 1963 Ph.D. Thesis, University of California, Berkeley.

Kawaguti, M. 1961 *J. Phys. Soc. Japan* **16**, 2307.

Moffatt, H. K. 1964 *J. Fluid Mech.* **18**, 1.

Maull, D. J. & East, L. F. 1963 *J. Fluid Mech.* **16**, 620.

Prandtl, L. 1904 *Proc. Third Intern. Math. Kongr. Heidelberg*, also *NACA Tech. Memo.* 452.

Snyder, L. J., Spriggs, J. W. & Stewart, W. E. 1964 *A.I.Ch.E. J.* **10**, 535.

Weiss, R. F. & Florsheim, B. H. 1965 *Phys. Fluids* **8**, 1631.

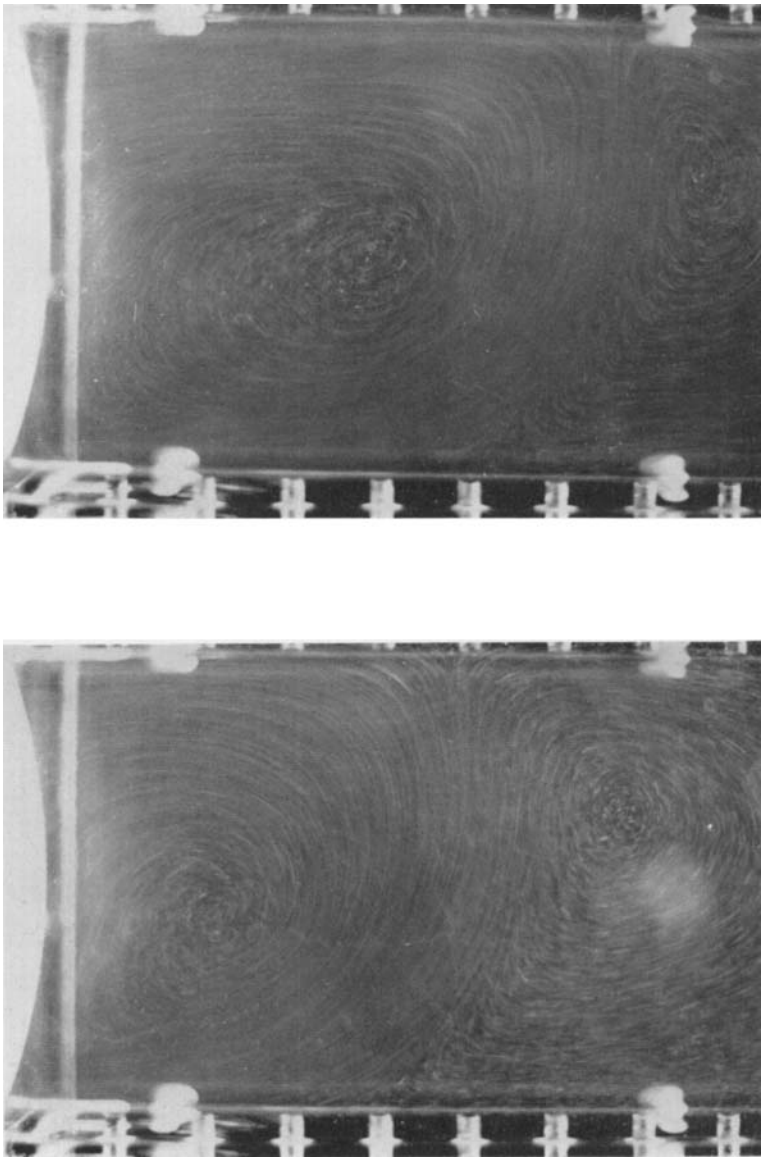

(*a*) $R = 840$ (*b*) $R = 2570$

FIGURE 5. Typical streamline patterns in an infinite cavity.

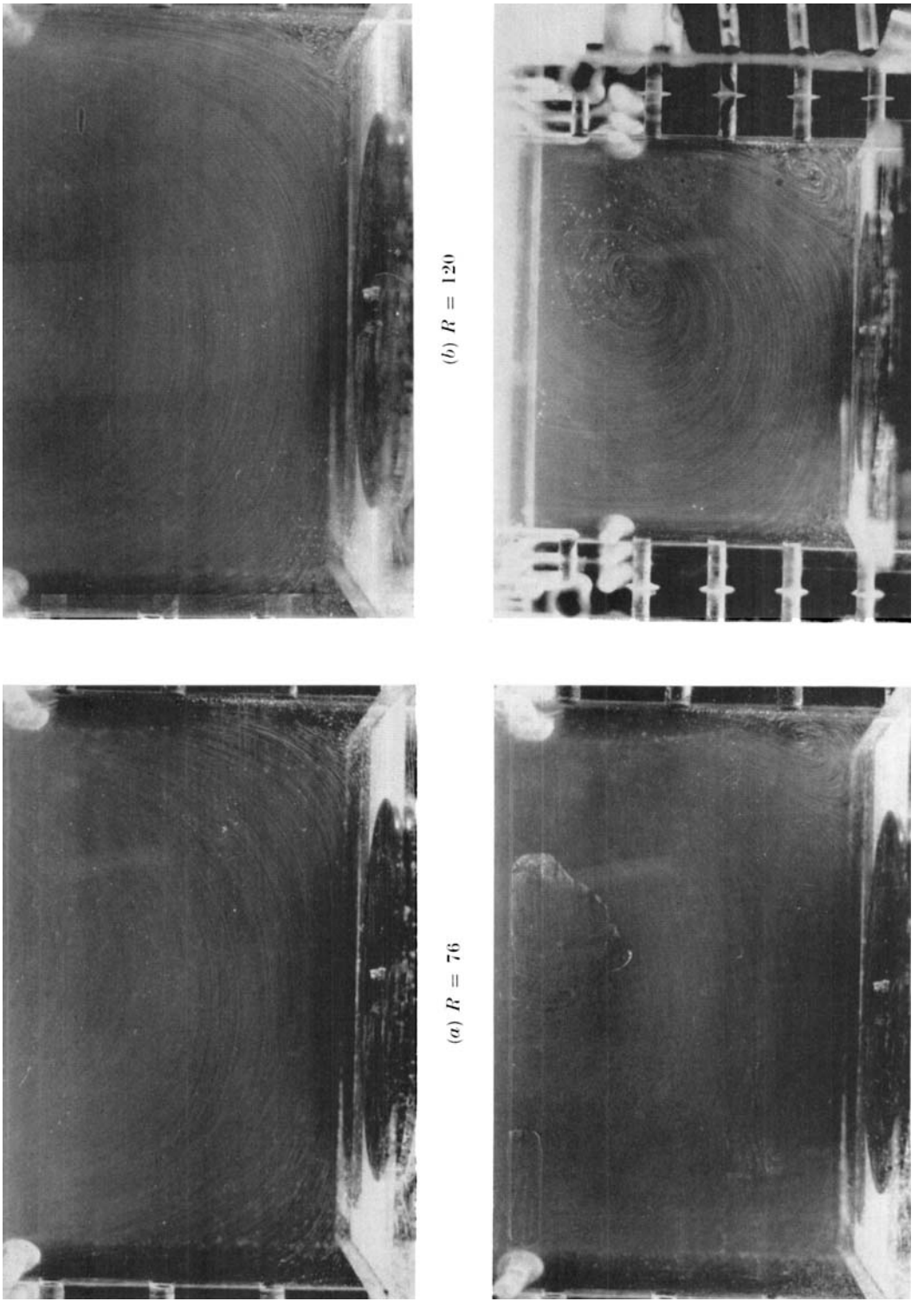

(*a*) $R = 76$ (*b*) $R = 120$

(*c*) $R = 255$ (*d*) $R = 470$

FIGURE 6. The growth of the corner vortex in a square cavity at low Reynolds number range (smaller than 500).

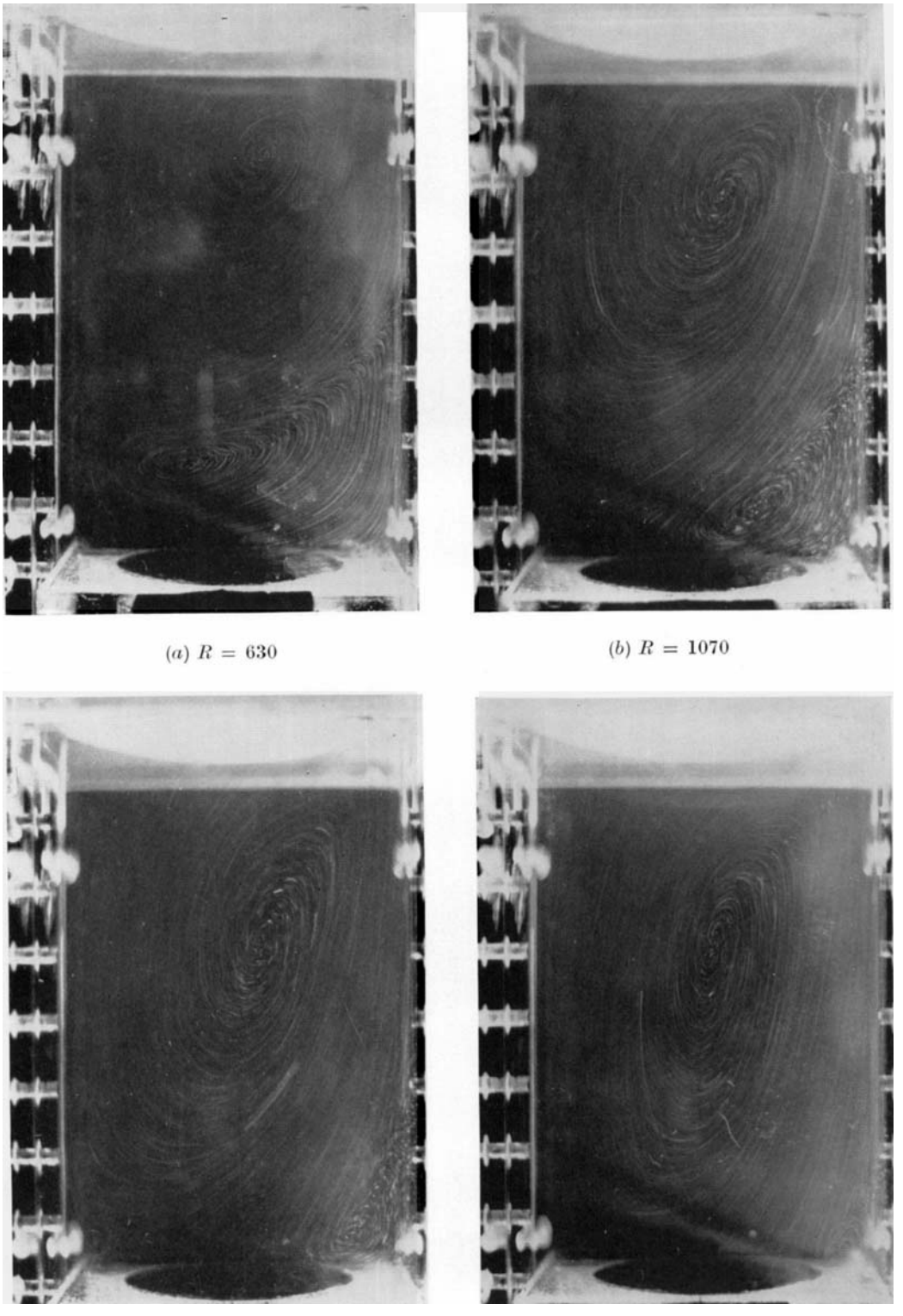

(*a*) $R = 630$ (*b*) $R = 1070$

(*c*) $R = 1330$ (*d*) $R = 2480$

FIGURE 8. The contraction of the secondary vortex into a small corner vortex at high Reynolds number ($A = 1{\cdot}6$).

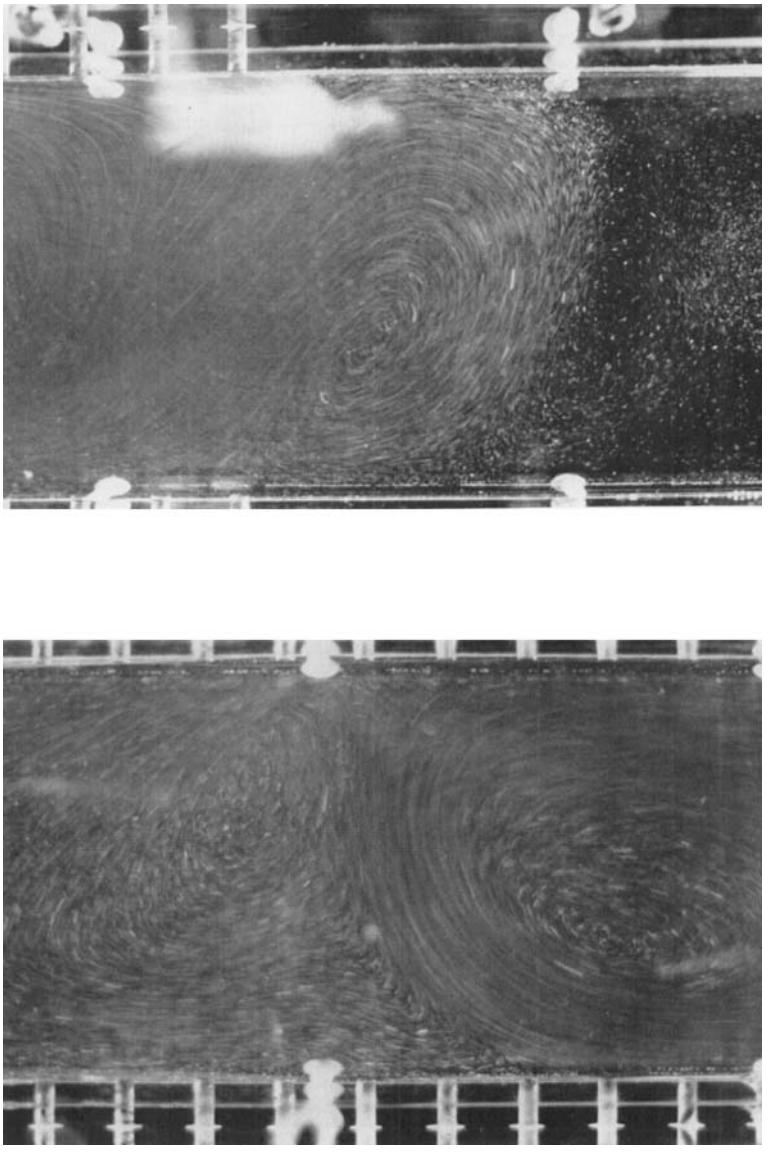

(*a*) First and second vortices (*c*) Third vortex

FIGURE 9. The first three vortices of the infinite cavity at Reynolds number 3200.